Mat Res Innovat (2002) 6:189–197
DOI 10.1007/s10019-002-0189-z

ORIGINAL ARTICLE

Seok Won Lee · Jae Ryoun Youn · Jae Chun Hyun

Prediction of fiber orientation structure for injection molded short fiber composites

Received: 3 January 2002 / Accepted: 15 January 2002 / Published online: 23 July 2002

Abstract Structure of fiber orientation in injection molded short fiber composites is predicted by the numerical analysis. To analyze the packing stage as well as the filling stage, a compressible generalized Hele-Shaw model is adopted. A numerical scheme free from coordinate transformation is developed for three-dimensional shell-like geometry. Flow-induced fiber orientation can be predicted by solving evolution equations for the orientation tensor with a suitable closure approximation. Fibers are mainly oriented toward the flow direction near the top cavity wall due to high shear rates, while they are randomly oriented near the centerline of cavity where low shear rates prevail. Thus, the molded parts show the skin-core structure of orientation. Structure of fiber orientation continues to change during the packing stage due to additional velocity gradients – which are likely to align fibers more towards the flow direction.

Keywords Fiber orientation · Short fiber composites · Injection molding · Packing stage · Numerical analysis · Orientation tensor · Skin-core structure

Introduction

It is essential for engineers to comprehend the relationships between processing, structure and properties. Short fiber reinforced composites, which are frequently injection-molded, are no exception and it will be very helpful if the relationships could be predicted.

Short fiber composites are used more widely because they not only are manufactured easily by processes such as injection molding and compression molding but also can retain some advantages of continuous fiber reinforced composites. During the processes, complex flow patterns are likely to happen in the cavity and to induce fiber orientation in a certain direction. Such flow-induced fiber orientation structure causes the molded part to show anisotropic properties and affects the final shape of the product. To obtain the part with desirable properties and precise shape, it is necessary to investigate the mechanism of flow-induced orientation. Thus, the relationship among processing, structure, and property of injection-molded short fiber composites can be understood.

After Jeffery's work [1] on the motion of ellipsoidal particles in Stokes flow of Newtonian fluid, many researchers have tried to predict flow-induced fiber orientation [2–5]. Tensor description of orientation structure [4] is now considered as a standard method for the mathematical description of fiber orientation. The evolution equation for the orientation tensor can be solved to predict flow-induced orientation if polymer-flow inside the cavity is known. Flow field inside the cavity is not easy to obtain because the geometry of the cavity is irregular. Thus, numerical approaches have been powerful tools in order to predict flow patterns inside the cavity [6–15]. So far only the polymer melt flow during filling stage of injection molding process has been analyzed. After the filling stage, however, packing of polymer melt occurs to compensate possible shrinkage of the final molded part. The packing stage is a dynamic process during which pressure in the cavity rises up to a maximum value and pressure field becomes uniform at almost every point inside the cavity. During the packing stage a significant flow of polymer inside the cavity may happen due to compressibility of the polymer melt under high packing pressure of the injection molding process [16–18]. Flow during the packing stage causes fibers to reorient, so that the structure of oriented fibers in the final part after the packing stage can be different from that at the end of the filling stage. Malzahn and Schultz [19] experimentally observed changes in the fiber orientation between almost at the end of the filling and after the packing stage. However, their study was qualitative, a quantitative comparison of the changes in the fiber orientation was not made

Seok Won Lee · Jae Ryoun Youn (✉)
School of Materials Science and Engineering,
Seoul National University, Seoul, Korea
e-mail: jaeryoun@gong.snu.ac.kr

Jae Chun Hyun
Department of Chemical Engineering, Korea University,
Seoul, Korea

and an explanation for the changes was not sufficient. A compressible flow during the filling stage may happen when the cavities are not symmetric or a multi-cavity mold is used. Several researchers have tried to analyze the flow-induced orientation in these cases [20–22]. A complete investigation of flow and fiber orientation at the packing stage has not been made yet.

In this study, structure of fiber orientation in the final molded part is predicted by the numerical procedure considering the packing as well as the filling stages. The equation of state of Tait [17–18, 20–22] is employed to describe the compressibility of the polymer melt. A modified Cross model is used to represent Non-Newtonian viscosity of the polymer melt. Pressure and temperature fields inside the cavity are obtained by the hybrid control volume finite element/finite difference method. Fiber orientation is predicted by solving the evolution equation of the orientation tensor from the given flow field.

Relation to previous work

Flow-induced fiber orientation results from the gradients of velocities. Therefore, the analysis of the filling stage in injection molding is considered as the prime subject in the prediction of fiber orientation in the final molded part. Givler et al. [2] calculated the changes in the fiber orientation angles for a simple flow situation. Jackson et al. [6] predicted changes in fiber orientation during the compression molding by calculating the two-dimensional orientation distribution function. However, the calculation of the orientation distribution function is so tedious that the solution is obtained only at a few prescribed positions in the cavity. Advani and Tucker III [7] calculated the two-dimensional 2nd order orientation tensor during the compression molding. The tensor description of fiber orientation makes the prediction of fiber orientation simple and compact. Altan et al. [8] and Henry De Frahan et al. [9] predicted the change in fiber orientation during injection molding by the finite difference method and finite element method, respectively. Only the filling stage was considered in their predictions. Bay and Tucker III [10–11] calculated the three-dimensional orientation tensor in the filling stage for the simple geometries of the strip and disk. They compared their numerical results with experimental ones. The skin-core structure of fiber orientation in the final part was confirmed. Indeed, the effect of shearing near the top surface of the cavity leads to the skin layer where fibers are largely oriented in the flow direction, and the effect of stretching flow near the centerline of cavity results in the core layer where fiber are largely oriented perpendicular to the flow direction. Ranganathan and Advani [12] performed an analysis of coupled flow and fiber orientation in the case of filling a cavity with simple geometry. But, as pointed by Tucker III [23], the coupled analysis of flow and fiber orientation is important only for the case of very high fiber volume fraction or thick cavity, which is not the usual case of injection molding. Ko and Youn [13] and Ko [14] analyzed the flow and fiber orientation in the thickness plane for injection molding considering the fountain flow effect. The skin layer of orientation in the final part seemed to be influenced by the fountain flow effect. But, for the case of irregular shape of the cavity, the consideration of the fountain flow cannot be dealt with easily. The coupled simulation of flow and fiber orientation for an arbitrary shaped cavity was performed by Chung and Kwon [15]. They predicted the broader core layer near the entrance, which is in better agreement with the experimental results. However, the predicted results are not in good agreement with the experimental results obtained for locations away from the entrance of the cavity. As mentioned above, Malzahn and Schultz [19] experimentally observed the change in fiber orientation between the element close to the end of the filling and after the packing. However, they have only presented SEM pictures of the sectioned plane of the final part. Any quantitative analyses were not made. Lee et al. [20], Lee [21], Lee and Youn [22] tried to consider effects of compressibility of polymer melt. The packing-induced flow affected the structure of fiber orientation in the final part. The core-layer became broader or narrower depending on the geometry of the cavity and processing conditions. They have only considered the compression of the polymer melt during the filling stage, which is likely to happen in the case of multi-cavity or asymmetrically shaped cavity.

As mentioned above, a velocity profile with considerable magnitude can be built-up during the packing stage due to high pressure inside the cavity. Thus, a complete analysis of the packing stage is necessary. Innovative in the present work is the prediction of the structure of fiber orientation in the injection molded short fiber composites expanded to the packing stage as well as the filling stage. An effective numerical scheme that is easy to implement and suitable for three-dimensional shell like geometry of the cavity will be also presented.

Numerical Analysis

Structure of fiber orientation in the molded part is directly related to the flow field inside the cavity. Once the flow field is obtained, the orientation field can be calculated through a proper procedure. Along with the equation of state and constitutive equations, continuity, momentum, and energy equations should be solved simultaneously to obtain the flow field. Tucker III [23] showed that the flow and fiber orientation fields can be decoupled as long as the gap between the top surface and the bottom surface is sufficiently small – which is true in most injection molding situation.

3.1 Flow Analysis

The coordinate system employed is shown in Fig. 1.

With the assumption of quasi-steady state, compressible, creeping, non-isothermal and inelastic flow, and for

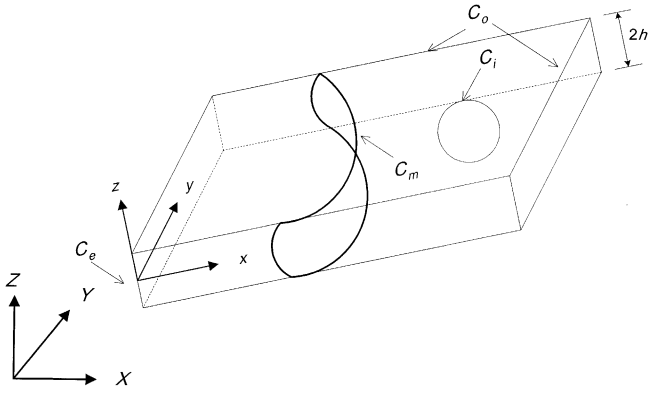

Fig. 1 Schematic presentation of the flow in the cavity and the definition of the coordinate system

the thin gap cavity, the governing equations for pressure and temperature can be simplified as follows:

$$G\frac{\partial p}{\partial t}-\frac{\partial}{\partial x}\left(\tilde{S}\frac{\partial p}{\partial x}\right)-\frac{\partial}{\partial y}\left(\tilde{S}\frac{\partial p}{\partial y}\right)=-F \tag{1}$$

$$\rho C_p\left(\frac{\partial T}{\partial t}+u\frac{\partial T}{\partial x}+v\frac{\partial T}{\partial y}\right)=k\frac{\partial^2 T}{\partial z^2}+\eta\dot{\gamma}^2 \tag{2}$$

where x, y, and z are the local Cartesian coordinates, and u and v are in-plane velocity components, p is pressure, T is temperature, ρ is density, C_p is heat capacity, k is thermal conductivity, η is viscosity, and $\dot{\gamma}$ is the magnitude of shear strain rate which can be calculated as:

$$\dot{\gamma}=\sqrt{\left(\frac{\partial u}{\partial z}\right)^2+\left(\frac{\partial v}{\partial z}\right)^2}=\frac{|z|}{\eta}\sqrt{\left(\frac{\partial p}{\partial x}\right)^2+\left(\frac{\partial p}{\partial y}\right)^2} \tag{3}$$

$\tilde{S}$, G and F are given as below.

$$\tilde{S}\equiv\int_0^h \rho\int_z^h\frac{\tilde{z}}{\eta}d\tilde{z}dz \tag{4}$$

$$G=\int_0^{\chi}\left(\frac{\partial\rho_l}{\partial p}\right)_T dz+\int_{\chi}^h\left(\frac{\partial\rho_s}{\partial p}\right)_T dz \tag{5}$$

$$F=\int_0^{\chi}\left(\frac{\partial\rho_l}{\partial T}\right)_p\frac{\partial T}{\partial t}dz+\int_{\chi}^h\left(\frac{\partial\rho_s}{\partial T}\right)_p\frac{\partial T}{\partial t}dz+(\rho_l-\rho_s)_{z=\chi}\frac{\partial\chi}{\partial t} \tag{6}$$

Here subscripts l and s represent liquid and solid phases, respectively, and χ is the location for the solid/liquid interface. $\tilde{S}$ is the fluidity, and G and F represent the dependence of density on pressure and temperature, respectively. The last term in Eq. (6) can be neglected if an amorphous polymer is used as the matrix. Nonslip conditions and the prescribed temperature condition at the top and the bottom cavity surfaces have been used to derive the above equations. Symmetric conditions at the centerline of the cavity are also implied. The detailed derivation of the above equations can be found in [20–22]. Boundary conditions for the Eq. (1) are

$$\begin{array}{ll}\text{at } C_m & p=0\\ \text{at } C_i \text{ or } C_o & \frac{\partial p}{\partial n}=0\\ \text{at } C_e & p=p_e(t)\end{array} \tag{7}$$

where n denoted the outward normal direction.

The state equation of Tait [17–18, 20–22] is employed to model the density of the polymer both in the liquid and in the solid phase.

$$v(T,p)=\frac{1}{\rho(T,p)}=v_0(T)\left[1-0.0894\ln\left(1+\frac{p}{B(T)}\right)\right] \tag{8}$$

where

$$v_0(T)=\begin{cases}b_{1,l}+b_{2,l}\bar{T} & (T>T_t)\\ b_{1,s}+b_{2,s}\bar{T} & (T<T_t)\end{cases} \tag{9}$$

$$B(T)=\begin{cases}b_{3,l}\exp(-b_{4,l}\bar{T}) & (T>T_t)\\ b_{3,s}\exp(-b_{4,s}\bar{T}) & (T<T_t)\end{cases} \tag{10}$$

$$\bar{T}\equiv T-b_5 \tag{11}$$

$$T_t(p)=b_5+b_6p \tag{12}$$

where b_i's are material constants.

The modified Cross model is used to describe the shear thinning behavior of the polymer melt:

$$\eta=\frac{\eta_0}{1+\left[\frac{\eta_0\dot{\gamma}}{\tau^*}\right]^{1-n}} \tag{13}$$

$$\eta_0=B\exp\left[\frac{T_b}{T}\right]\exp(\beta p) \tag{14}$$

where B, T_b, β, τ^*, and n are material constants.

Governing equations for pressure can be solved by the control-volume finite element method (CVFEM). In this method the pressure field is determined in order to satisfy the conservation law, which is evaluated from the flux across the control-volume boundary. Because the equation has the same form as the diffusion equation, it can be solved without a coordinate transformation, although the geometry is three-dimensionally shaped thin shell. Figure 2(a) shows the elements and their definition of control volume and Fig. 2(b) shows one typical element among them. A control volume is made up by the assembly of sub-control volumes that share the same node. A sub-control volume is defined by connecting the centroid of the element to the mid-side boundaries of each element. Therefore, three sub-control volumes can be made in each element.

By assuming $\tilde{S}$, G and F to be constant in each element and integrating Eq. (1) over the control-volume containing node 1 in Fig. 2(b), the following equation can be obtained.

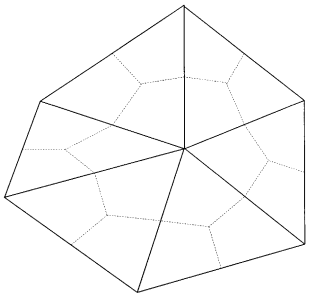

(a)

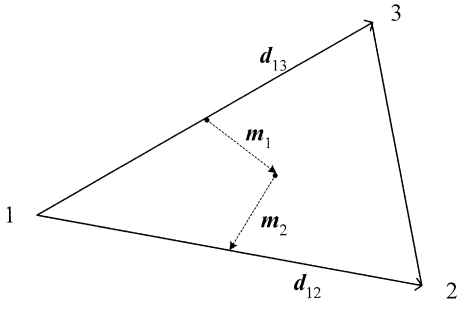

(b)

Fig. 2 Triangular finite elements and control volumes. (a) An assembly of elements and the definition of a control volume. (b) Single finite element and a sub-control volume associated with node 1

$$\sum_e G_e \frac{p_1^{t+\Delta t} - p_1^t}{\Delta t} \frac{A_e}{3} = \sum_e \int_{\Gamma_e} \tilde{S}_e \nabla p \cdot n \, d\Gamma_e - \sum_e F_e \frac{A_e}{3} \tag{15}$$

Here subscript e represents an element, Γ the boundaries of control volume in each element, and A the area of each element. If the pressure is assumed to vary linearly in the element, the gradient of pressure can be expressed [24] as:

$$\nabla p = -\frac{(p_3 - p_1) d_{12}^+ - (p_2 - p_1) d_{13}^+}{2A_e} \tag{16}$$

where the superscript + means the vector is rotated clockwise by the angle $\pi/2$ along the plane. Let m be the vector that is normal to the boundary of sub-control volume and has the same length as the sub-control volume boundary:

$$m = -(m_1^+ + m_2^+) = -\frac{1}{2}(d_{12}^+ - d_{13}^+) \tag{17}$$

Then the surface integration term of Eq. (15) can be evaluated as below.

$$\int_\Gamma \tilde{S}_e \nabla p \cdot n \, d\Gamma = \tilde{S}_e \nabla p \cdot m = \frac{\tilde{S}_e}{4A_e} \left[p_3 d_{12} \cdot d_{32} + p_2 d_{13} \cdot d_{23} + p_1 |d_{23}|^2 \right] \tag{18}$$

The relation of $\mathbf{a}^+ \cdot \mathbf{b}^+ = \mathbf{a} \cdot \mathbf{b}$ is used in the above derivation. Finally, substitution of Eq. (18) into Eq. (15) leads to:

$$p_1^{t+\Delta t} = \frac{\sum_e a_{2e} p_{2e}^{t+\Delta t} + \sum_e a_{3e} p_{3e}^{t+\Delta t} + \sum_e a_{4e}}{\sum_e a_{1e}} \tag{19}$$

where

$$a_{1e} = \frac{G_e A_e}{3} + \frac{\tilde{S}_e \Delta t}{4A_e} |d_{23}|^2 \tag{20}$$

$$a_{2e} = \frac{\tilde{S}_e \Delta t}{4A_e} d_{13} \cdot d_{23} \tag{21}$$

$$a_{3e} = \frac{\tilde{S}_e \Delta t}{4A_e} d_{12} \cdot d_{32} \tag{22}$$

$$a_{4e} = \left(G_e p_1^t - F_e \Delta t \right) \frac{A_e}{3} \tag{23}$$

Node-by-node iterations make it possible to obtain the pressure field and neither stiffness matrix nor coordinate transformation is necessary. An under-relaxation procedure will be helpful to improve the convergence if a significant non-linearity is present.

Equation (2) which governs the temperature field is solved by the help of the finite difference method with a suitable upwind scheme to ensure numerical stability [17, 21, 22]. An implicit time stepping is implemented to remove the restriction in determining time step. The temperature field is obtained at the centroid of elements. Detailed formulation is given in the reference [21]. Equations (2)and(19) are strongly coupled, so they should be solved iteratively.

The melt front is advanced by the control volume method [17, 21, 22]. The fill factor at each node, f, is defined as the ratio of the amount of the polymer melt within the control volume to the amount that the control volume is able to hold. Governing equations apply only to the filled region ($f = 1$). After the pressure and temperature fields are obtained, fill factors for the partially filled region ($0 < f < 1$) are updated. The time step is selected so that only one control volume should be filled at each time step. The method has an advantage in dealing with a geometrically complex cavity or a case of multiple melt fronts. Pressure at the gate $p_e(t)$ is then determined to give the constant volume flow rate which is specified as an input.

3.2 Fiber orientation prediction

Structure of fiber orientation is described by using the second order orientation tensors. The tensorial representation of orientation state has an advantage of reducing the amount of computation significantly as well as its normality and symmetry [4]. The second and fourth order orientation tensors are defined as follows:

$$a_{ij} = \int p_i p_j \psi(p) dp \tag{24}$$

$$a_{ijkl} = \int p_i p_j p_k p_l \psi(p) dp \tag{25}$$

where p denotes the unit vector in the fiber direction (Fig. 3) and ψ is the orientation distribution function defined as below.

$$P(\theta_0 \le \theta \le \theta_0 + d\theta, \phi_0 \le \phi \le \phi_0 + d\phi) = \psi(\theta_0, \phi_0) \sin\theta_0 d\theta d\phi \tag{26}$$

To predict the change of orientation tensors induced by the flow inside the cavity, an evolution equation for orientation tensor should be solved [4].

$$\frac{Da_{ij}}{Dt} = -\frac{1}{2}(\omega_{ik}a_{kj} - a_{ik}\omega_{kj}) + \frac{1}{2}\lambda(\dot{\gamma}_{ik}a_{kj} + a_{ik}\dot{\gamma}_{kj} - 2\dot{\gamma}_{kl}a_{ijkl}) + 2C_I\dot{\gamma}(\delta_{ij} - 3a_{ij}) \tag{27}$$

where $\lambda = (r_e^2 - 1)/(r_e^2 + 1)$, C_I is the interaction coefficient proposed by Folgar and Tucker III [3], r_e is the aspect ratio of the short fiber, ω_{ij} is the vorticity tensor, and $\dot{\gamma}_{ij}$ is the shear rate tensor. The fourth order tensors appear in the above equations and should be expressed in terms of the second order orientation tensors to avoid recurrence. To meet this purpose, hybrid closure approximation suggested by Advani and Tucker III [5] is applied. The fourth order Runge-Kutta method with upwind scheme for convective terms is employed to solve Eq. (27) so that numerical stability should be insured [14, 21].

Results and Discussion

Two cases of different cavities, a planar rectangular shaped cavity and a planar cavity with a rib, are investigated. The material used in the numerical simulation is polystyrene filled with carbon fibers. Constants of the modified Cross model for polystyrene [18] are given in Table 1. Thermal properties for polystyrene [25] and processing conditions are shown in Table 2. Inlet temperature and wall temperature are the same in both cases. Constants of the Tait state equation for polystyrene are listed in Table 3 [18]. Initial random orientation is assumed at the gate and C_I is set to 0.001 in both cases. Constant flow rate which results in the fill time of 0.997 sec is specified at the gate.

4.1 Planar Rectangular Cavity

A simple shaped planar rectangular cavity (20 × 4 × 0.2 cm) is tested by the numerical simulation. Geometry, its finite element mesh, and location of the gate are shown in Fig. 4. A fan gate which has the same thickness as the cavity and the length of 2 cm is located at the entrance of the cavity. The constant flow rate at the gate is specified as 16.80 cm³/s so that the fill time should be 0.997 s. The packing pressure is set to be 60 MPa. The packing time, which is defined as the time at which pressure at the gate reaches the specified packing pressure, is calculated as 1.014 s.

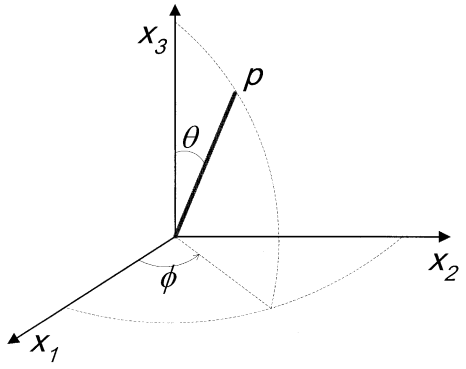

Fig. 3 Position vector of an oriented fiber

Table 1 Constants of the modified Cross model for polystyrene

n	τ/(dyne/cm²)	B/(poise)	T_b/(K)	β/(cm²/dyne)
0.274	2.31×10^5	3.04×10^{-8}	13300	3.5×10^{-9}

Table 2 Thermal properties of polystyrene and molding conditions

K/(erg/cm·K·s)	C_p/(erg/g·K)	T_{gate}/(K)	T_{wall}/(K)	t_{fill}/(s)
9.8×10^3	2.4×10^7	473	333	0.997

Table 3 Constants for the Tait state equation for polystyrene

$b_{1,l}$/(cm³/g)	0.988
$b_{2,l}$/(cm³/g·K)	6.10×10^{-4}
$b_{3,l}$/(dyne/cm²)	115.0×10^7
$b_{4,l}$/(K⁻¹)	3.66×10^{-3}
$b_{1,s}$/(cm³/g)	0.988
$b_{2,s}$/(cm³/g·K)	1.49×10^{-4}
$b_{3,s}$/(dyne/cm²)	238.0×10^7
$b_{4,s}$/(K⁻¹)	2.10×10^{-3}
b_5/(K)	385.0
b_6/(cm²·K/dyne)	7.8×10^{-7}

Flow inside the planar rectangular cavity can be thought to be almost one-dimensional and the predicted melt front advancement reflects the fact well as illustrated in Fig. 5. Due to compressibility of the polymer melt under high pressure, a significant velocity develops even in the packing stage. Figure 6 shows the gapwise averaged velocity vectors and pressure distribution at the end of the packing stage. It can be seen that a very large velocity occurs especially near the gate region during packing.

An orientation tensor has three principal axes whose magnitudes are the corresponding eigenvalues. To visualize orientation states in the final part, an orientation cross can be defined as the assembly of three lines which have the directions of eigenvectors and the lengths of eigenvalues by using the above mentioned facts. Orientation tensors are obtained at the centroid of each element with respect to the thickness direction and orientation crosses can be so obtained as well. If fibers are strongly oriented in one direction, an orientation cross will appear as if it were a single line. If fibers are randomly oriented,

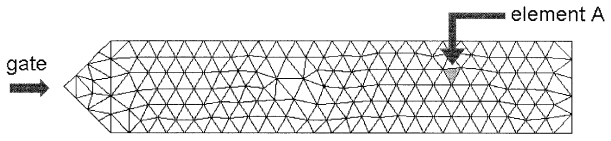

Fig. 4 Geometry and its finite element configuration for the planar rectangular cavity

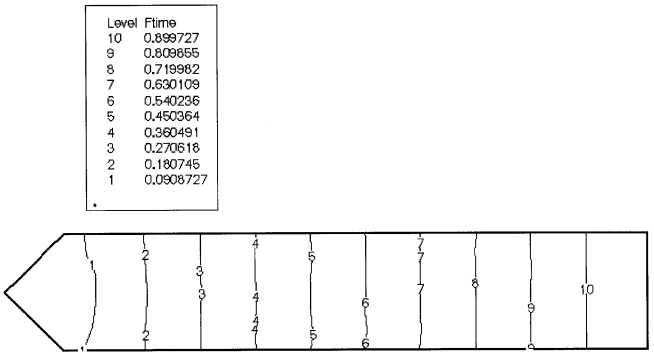

Fig. 5 Predicted melt front advancement with respect to time for the planar rectangular cavity

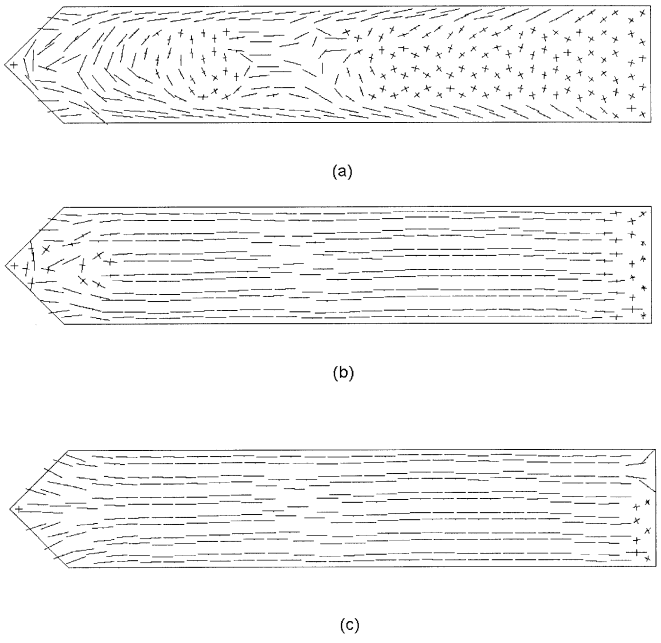

Fig. 7 Predicted orientation states at the end of packing stage for the planar rectangular cavity (a) at z/h=0.0, (b) at z/h=0.4, and (c) at z/h=0.9

Fig. 6 Pressure (dyne/cm^2) distribution and gapwise averaged velocity vectors at the end of packing stage for the planar rectangular cavity

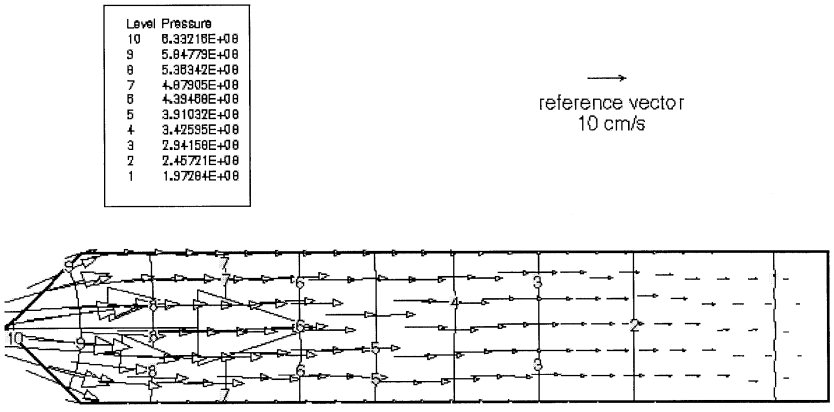

an orientation cross will appear as the assembly of three orthogonal lines that have the same length. Orientation states in the planar rectangular cavity after the packing stage are visualized in Fig. 7 which is the projection of the orientation crosses into the x-y plane. While random states of fiber orientation occur along the centerline of the cavity (Fig. 7(a)), most fibers are oriented in the flow direction near the top cavity wall (Fig. 7(c)). The random orientation states near the centerline are due to low shear rates. On the other hand, high shear rates near the top cavity wall cause a fiber orientation to be developed in the flow direction. Thus, the final molded-part has a skin-core structure of fiber orientation which represents well-developed orientation in the flow direction near the top and bottom cavity walls and less-developed orientation near the centerline of the cavity. This skin-core structure can be examined further in Fig. 8 which shows changes in the value of the orientation tensor components with respect to the thickness direction at the element A shown in Fig. 4. It can be clearly seen that the skin-core structure exists from the fact that the component a_{11} is the descriptor of magnitude of fiber orientation in the 1-direction. The thickness of the skin layer is slightly larger than that of the core layer. The low value of a_{12} means that the principal axes of orientation are not tilted in the x-y plane.

4.2 Cavity With a Rib

A rectangular cavity ($12 \times 8 \times 0.2$ cm^3) with a rib whose height is 1 cm and thickness is the same as the cavity has also been tested by numerical simulations. The geometry and its finite element configuration are shown in

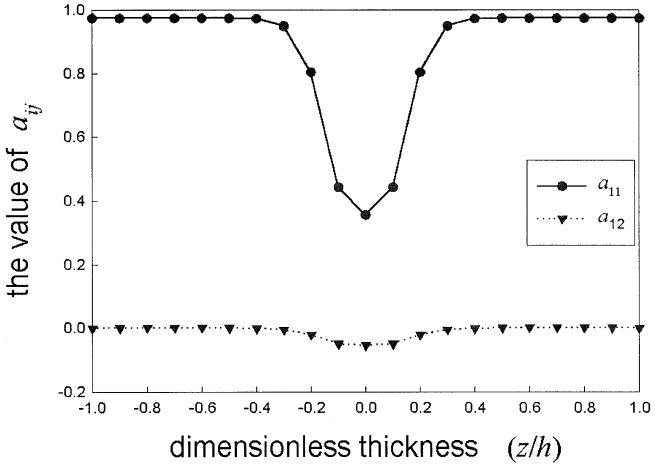

Fig. 8 Components of the orientation tensor at the element A after packing stage for the planar rectangular cavity, which shows the skin-core structure of fiber orientation

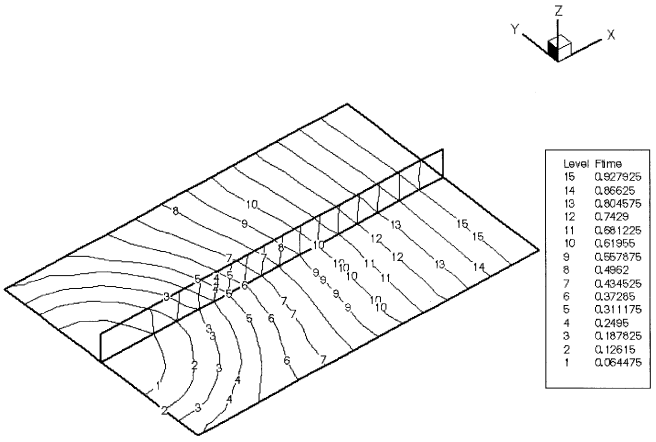

Fig. 10 Predicted melt front advancement with respect to time for the cavity with the rib

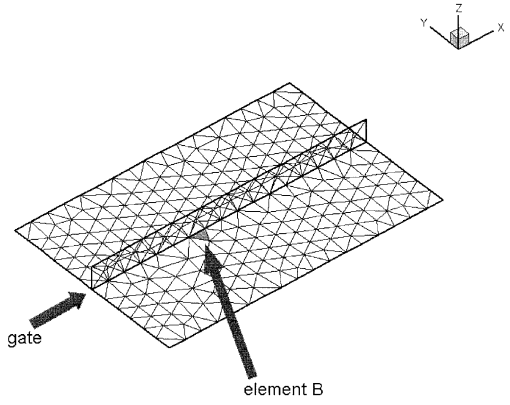

Fig. 9 Geometry and its finite element configuration for the cavity with the rib

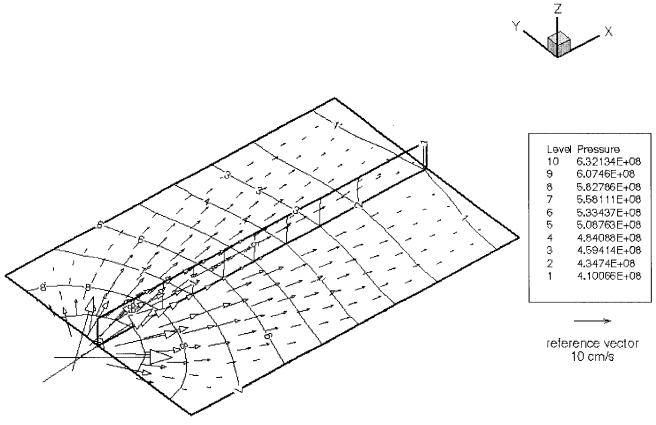

Fig. 11 Pressure (dyne/cm^2) distribution and gapwise averaged velocity vectors at the end of packing stage for the cavity with the rib

Fig. 9. Since the shape of the cavity is like a three-dimensional shell, coordinate transformation will be inevitable if the conventional finite element method, other than the control volume finite element method mentioned above, is used. The constant flow rate of 21.60 cm^3/s is specified at the gate. The fill time is 0.997 s which is the same as the previous case. The packing pressure of 45 MPa is set at the gate and the packing time is calculated as 1.036 s.

The melt front advancement during the filling stage is illustrated in Fig. 10. In the beginning, flow spreads in a nearly circular shape. Then, the melt front becomes flat as the cavity is filled. Figure 11 shows the gapwise averaged velocity vectors and pressure distribution at the end of the packing stage. Considerable velocity field is also formed near the gate in this case.

Predicted orientation states in the final molded part are shown in Fig. 12. Like the previous case, fibers are rather randomly oriented near the centerline of the cavity and fibers are well oriented in the flow direction near the top cavity wall. Usually a rib is designed to prevent the part from warping along the longer direction. In order to reduce the amount of warpage, the modulus along the longer direction should be high. From that point of view, it may be proposed that the rib performs better when the direction of the rib is parallel to the flow direction than when the direction of the rib is transverse to the flow direction.

To check the effect of the packing on the structure of fiber orientation, changes in orientation tensor components between after the filling stage and after the packing stage are compared in Fig. 13. It can be seen that the value of a_{11} becomes higher after the packing stage in the region between the core and skin layers, which means fibers are more aligned toward the flow direction due to the flow developed during the packing stage. Similarly, the value of a_{12} becomes lower in that region, where the principal axes of fiber orientation become less tilted in the x-y plane. Flow generated by the compressibility of the polymer melt during the packing stage is the source of changes in the structure of fiber orientation. Figure 14 shows velocity profile with respect to the thickness di-

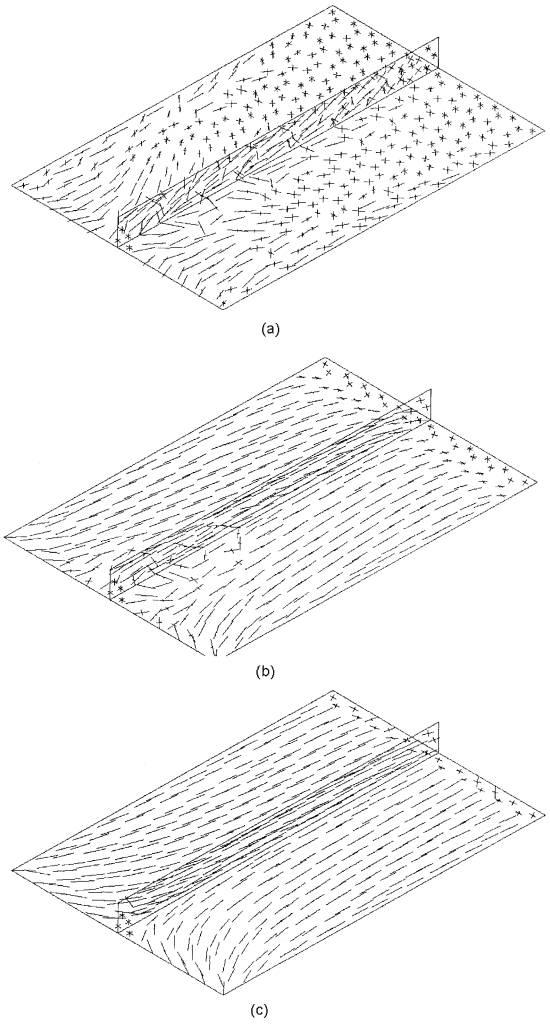

Fig. 12 Predicted orientation states at the end of packing stage for the cavity with the rib (a) at z/h=0.0, (b) at z/h=0.4, and (c) at z/h=0.9

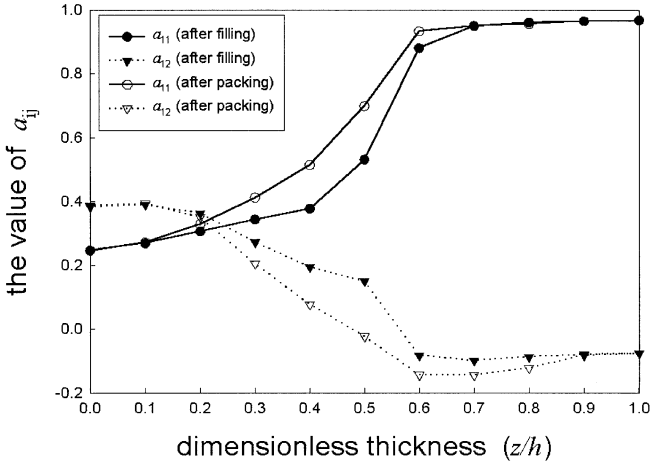

Fig. 13 Changes in predicted fiber orientation at the element B between after filling stage and after packing stage

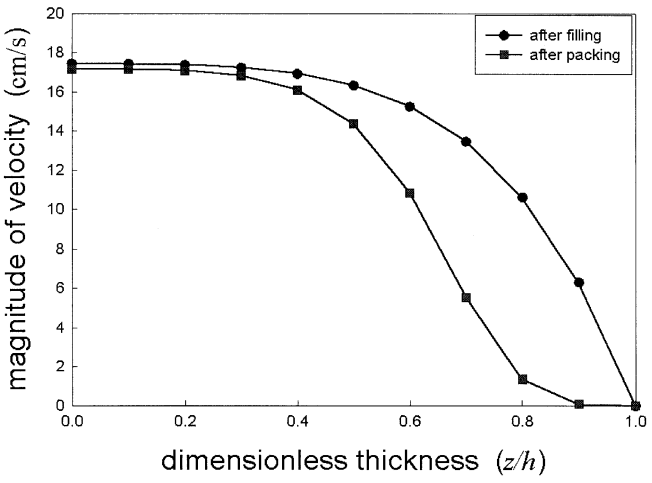

Fig. 14. Comparison of velocity profile with respect to the thickness direction between after filling stage and after packing stage

rection just after the filling stage and just after the packing stage. The magnitude of velocity profile at the end of the packing stage is comparable with that at the end of the filling stage. The additional velocity gradients force fibers to keep orienting in the flow direction during packing.

Concluding remarks

We have developed a numerical scheme for the general three-dimensional shell-like geometry, which does not require coordinate transformations. Tait's state equation is adopted to describe compressibility and modified Cross model is employed to consider non-Newtonian behavior of the polymer melt. Heat transfer and phase change due to cooling by the relatively cold mold wall are also considered. The 2nd order orientation tensor is introduced to describe 3-dimensional states of fiber orientation. It is possible to predict flow-induced fiber orientation by solving the evolution equation for the orientation tensor with a suitable closure approximation. Flow and temperature fields are obtained by the hybrid CVFEM/FDM technique. Melt front is advanced by control volume method. Orientation fields are solved by the 4th order Runge-Kutta method.

We have found that fibers are mainly oriented toward the flow direction near the top and/or bottom cavity wall due to high shear rates. On the other hand, the fibers are rather randomly oriented near the centerline of the cavity due to low shear rates in that region. Thus, the structure of skin-core type occurs throughout the thickness direction of the final molded part. The flow-induced fiber orientation pattern will result in anisotropic properties of the part. The fiber orientation structure in the part continues to change during the packing stage due to additional velocity gradients induced by the compressibility of polymer melt. These additional velocity gradients will make fibers aligned further along the flow direction in

the local region between the skin layer and the core layer. A comparison with experimental results should be done, but the experimental determination of three-dimensional orientation is not dealt with easily. Developing a general way of determining three-dimensional orientation and enhancing the prediction of fiber orientation will be the future research subject.

Acknowledgements This study was supported by research grants from the Korea Science and Engineering Foundation (KOSEF), Seoul, through the Applied Rheology Center at the National University of Korea. The authors are grateful for this support.

References

1. Jeffery GB (1923) Proc royal soc A 102: 161
2. Givler RC, Crochet MJ, Pipes RB (1983) J compos mater 17: 330
3. Folgar F, Tucker III CL (1984) J reinf plast compos 3: 98
4. Advani SG, Tucker III CL (1987) J rheol 31: 751
5. Advani SG, Tucker III CL (1990) J rheol 34: 367
6. Jackson WC, Advani SG, Tucker III CL (1986) J compos mater 20: 539
7. Advani SG, Tucker III CL (1990) Polymer compos 11: 164
8. Altan MC, Subbiah S, Güçeri SI, Pipes RB (1990) Polymer eng & sci 30: 848
9. Henry De Frahan H, Verleye V, Dupret F, Crochet MJ (1992) Polymer eng & sci 32: 254
10. Bay RS, Tucker III CL (1992) Polymer compos 13: 317
11. Bay RS, Tucker III CL (1992) Polymer compos 13: 332
12. Ranganathan S, Advani SG (1993) J non-newtonian fluid mech 47: 107
13. Ko J, Youn JR (1995) Polymer compos 16: 114
14. Ko J (1994) PhD Thesis, Kaist, Taejon, Korea
15. Chung ST, Kwon TH (1995) Polymer eng & sci 35: 604
16. Hieber CA (1987) Melt-viscosity characterization and its application to injection molding. In: Isayev AI (ed) Injection molding and compression molding fundamentals. Marcel Dekker, New York, pp 61–78
17. Chiang HH, Hieber CA, Wang KK (1991) Polymer eng & sci 31: 116
18. Chiang HH, Hieber CA, Wang KK (1991) Polymer eng & sci 31: 125
19. Malzahn JC, Schultz JM (1986) Compos sci & tech 25: 187
20. Lee SC, Yang DY, Ko J, Youn JR (1997) J mater process technol 70: 83
21. Lee SW (1997) MS Thesis, Seoul National University, Seoul, Korea
22. Lee SW, Youn JR (1999) Macromol symp 148: 211
23. Tucker III CL (1991) J non-newtonian fluid mech 39: 239
24. Winslow AM (1967) J comput phys 2: 149
25. Kuo Y, Kamal MR (1976) AIChE j 22: 661